Flexural response of concrete-filled seamless steel tubes

Farid H. Abed [a],*, Yosri I. Abdelmageed [a], A. Kerim Ilgun [b]

[a] *Department of Civil Engineering, American University of Sharjah, Sharjah 26666, United Arab Emirates*
[b] *Department of Civil Engineering, Karatay University, Konya, Turkey*

A R T I C L E   I N F O

A B S T R A C T

This paper aims to investigate the flexural behavior of concrete filled tubes (CFSTs) made of seamless steel which can handle more pressure than welded steel. Experimental, Theoretical and Finite Element Analyses are utilized for this purpose. The experimental program consists of four-point bending tests of six CFSTs and three hollow steel tubes (STs) for three different Diameter-to-thickness (D/t) ratios of 7.82, 13.5 and 17.5. The test results included are the moment versus displacement and strains, failure modes and ultimate capacities. The contribution of the concrete infill to the flexural capacity was more significant in specimens with higher D/t ratios. All CFST beams exhibited ductile mode of failure with no local buckling. The experimental moments are compared to theoretical nominal moments calculated by well-known international design codes such as the Architectural Institute of Japan (AIJ), the British Standard (BS), the AISC-LRFD, and the Euro code4. Only the AIJ equations predicted non-conservative capacities particularly at the highest D/t ratio. The other codes and standards were more conservative since they did not consider the effect of concrete confinement in their design equations. Finite Element (FE) simulation of the flexural response of CFST is also conducted by developing a nonlinear 3D model considering both material and geometric nonlinearities. The FE model is verified using the present experimental results and a good agreement was achieved in terms of the moment capacity, the failure mode and the moment-mid span deflection curves. In addition, the verified finite element model was used to carry out a parametric study considering wider ranges of D/t ratios and yield strengths.

© 2018 Elsevier Ltd. All rights reserved.

1. Introduction

Concrete-filled steel tubes (CFSTs) are composite structural members constituting of a steel tube and a concrete infill. Both materials mutually contribute to carrying the load and providing the necessary member stiffness where the steel tube improves the carrying capacity of the concrete and the concrete core delays the global and local buckling of the steel tube [1–3]. In current construction practice, CFSTs are commonly used as columns and braces in tall buildings, bridges and military facilities due to their large axial load capacity, compression stiffness and high deformation capacity [1, 4–7]. The flexural behavior of CFSTs is currently the prompt of much research and investigation. To date, the application of CFST in beams is limited. CFST members are currently employed in lofty structures as well as structures in earthquake-prone areas. Other applications include bridges and piers [1].

CFST members have the potential to combat various limitations of conventional reinforced concrete members. They enhance compression behavior since the concrete infill is well confined inside the steel tube,

which allows steel yielding before concrete crushing. The confinement on concrete inside the steel tube also establishes a triaxial state of compression, which results in increased strength and strain of concrete [1]. Moreover, CFST is characterized by high strength and high ductility, which are contributed by the steel, as well as high load-carrying capacity, which is contributed by concrete [8]. Furthermore, the steel tubes readily provide formwork for concrete and hence, no additional formwork is required. This in return accelerates the construction process [9–11].

Considering the aforementioned multiple advantages, CFST is a promising structural element and hence, vast research efforts have been expended to investigate its mechanical properties, as well as its behavior in different applications. More specifically, recent research sheds light on the flexural behavior of CFST, to expand and develop the application of CFST in structures. Han tested 16 CFST beams with square and rectangular cross-sections to study their flexural behavior [3]. The concrete cube strength for these CFST beams ranged from 27 MPa to 40 MPa, and steel yield strength from 294 MPa to 330 MPa. Han also compared experimental ultimate moments of CFST beams with theoretical results calculated by codes equations including the Architectural Institute of Japan (AIJ) [16], the AISC-LRFD [12], the British Standard (BS) [13], and the Euro code [14]. It was found that flexural capacities obtained using these codes were conservative; with >20%

* Corresponding author.
E-mail addresses: fabed@aus.edu (F.H. Abed), b00069726@aus.edu (Y.I. Abdelmageed), kerim.ilgun@karatay.edu.tr (A. Kerim Ilgun).

prediction difference using AIJ and AISC, 12% difference using BS5400 (1979) and around 10% overestimation using EuroCode4. In addition, Han [3] developed two different analytical relationships, one for rectangular and the other for circular cross-sections, based on composite mechanics equations and regression analysis to predict the flexural capacities of CFST beams. It was mentioned that cooling of the weld produces residual stresses which can be up to 20% of yielding stress in the compression zone and full yielding stress in the tension one. All of the theoretical calculations do not account for these residual stresses which will lead to inaccurate flexural capacities. However, seamless tubes considered in this study do not have residual stresses since the steel tube were extracted from steel forms, without any welding.

Probst et al. [4] tested four 6-meter length CFST specimens with rectangular and circular cross-sections, and also with and without shear connections. The D/t ratio for their circular CFST specimens was 36 and the concrete strength was 22 MPa. The experimental ultimate moments for circular CFST beams without shear connection were compared to the AISC and EuroCode4, and both codes were found to be un-conservative. They suspect that the large diameter of concrete is the reason for this deviation from the codes since the effect of concrete shrinkage would be significant. Further research, with various D/t ratios, was recommended to investigate the applicability of AISC and EuroCode4 for calculating the flexural capacity of circular CFST beams.

Elchalakani et al. [15] investigated the flexural behavior of circular CFST beams with a range of D/t ratios between 12 and 110. It was found that local buckling does not occur for CFST specimens that have D/t ratio less than or equal to 40. According to their results, design of CFST using the AISC, AIJ, and EC4 codes was found to be un-conservative for the case of the low D/t ratios 12.8. This could be due to overestimating the CFST flexural capacity when more steel thickness is used.

Finite Element (FE) Analysis was also used by some researchers to investigate the flexural behavior of CFST members. For example, Moon et al. [1] studied the effect of the steel yield stress to the concrete compressive strength ($f_y/f_{c'}$), and the diameter to depth ratios (D/t) on the flexural behavior of circular CFST beams by developing a nonlinear FE model. They concluded that the $f_y/f_{c'}$ ratio improved the flexural capacity, while the D/t ratio has no significant effect. Wang et al. [16] also developed a nonlinear FE model to understand the flexural behavior of rectangular CFST beams. They compared the FE results with the data from previous experimental programs of 70 beam specimens. The moment capacities, the failure modes and the load vs displacement curves predicted by the FE model compared well with their experimental counterparts [16].

A thorough understanding of the flexural behavior of CFST beams is crucial to expand their application. The aim of this paper is to study the flexural behavior of circular CFST beams using seamless steel tubes and also considering a range of low D/t ratios between 7.82 and 17.5. This paper will also investigate the applicability of theoretical results predicted by international design codes such as AIJ, AISC, BS, and EC4, and determine if the conclusions made by the previous studies is applicable for seamless steel tubes. Finally, a three-dimensional finite element model capable of simulating the flexural response and predicting the ultimate capacity of CFST and ST beams will be developed using the commercial software ABAQUS by considering both material and geometric nonlinearities.

2. Experimental program

The experimental program of this study consisted of four-point bending tests of six CFSTs and three hollow steel tubes (STs). All steel tubes had the same diameter of 114 mm and length of 1100 mm; however, their thickness varied from 6.5 mm to 14.5 mm, resulted in three different D/t ratios. The specimens were placed in three groups based on their resulting D/t ratios. At each D/t ratio, two steel tubes were filled
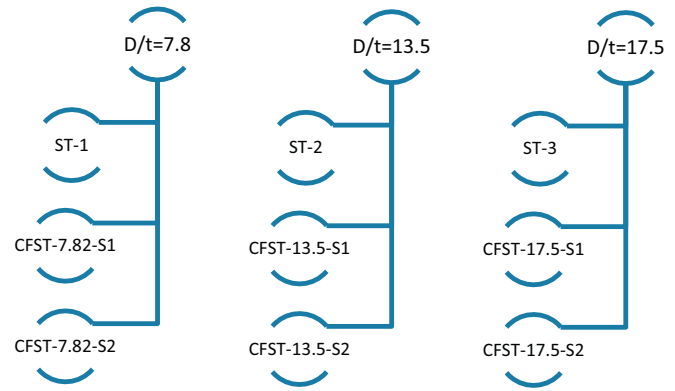

Fig. 1. Experimental program.

with normal concrete and one was left hollow. Fig. 1 illustrates the experimental program matrix used in this study.

Table 1 summarizes the concrete mix propositions used in this study. Three cubes and three cylinders were casted and tested after 28 days curing. The average compressive strength of the concrete infill was 43 MPa for cubes and 39.4 MPa for cylinders.

The steel tubes were readily produced by the manufacturer as seamless tubes. Thus, their diameters and thicknesses were fixed. Coupon specimens were manufactured and tested to extract the tensile stress-strain curve for each tube thickness as shown in Fig. 2. Accordingly, the average yield stress was 245 MPa with a corresponding yield strain of 0.001225 and the modulus of elasticity was around 200 GPa. In addition, the ultimate stress was about 530 MPa, which is more than twice the yield stress. The effect of such high strain hardening on the CFSTs flexural behavior was evident as will be discussed later.

CFST beam specimens were casted and compacted manually to ensure that concrete is distributed throughout the whole beam and is well confined inside the steel tube. The specimens were tested over a 1000 mm clear span in a four-point bending setup with a constant moment region of 400 mm, as shown in Fig. 3. The load was induced using a Universal Testing Machines (UTM), which has a load capacity of 1200 KN, and transferred to two loading points on the specimen through a spreader beam. The load was applied at a constant rate of 2 mm/min.

The mid-span deflection of each specimen was captured throughout the test using a linear variable displacement transducer (LVDT) located at the beam soffit. Strain gauges were also mounted at the center of the beams to measure the strain in both lateral and longitudinal directions. The load, mid-span deflection, and strains were recorded every 0.1 s using a high-speed data acquisition system. Moreover, special supports were used to hold the beams in place. The supports provided good grip of the circular test beams and prevented rotation. Fig. 3-b provides a depiction of the supports employed in this experiment.

3. Results and discussions

The experimental program was capable of capturing the behavior of the seamless CFSTs in term of their moment capacities at yield and at ultimate, their deformation behavior beyond the yield point and their failure modes.

Table 1
Concrete mix proportions.

Concrete type	Mix proportions (divided by the weight of cement)				
	Cement	Fly ash	Coarse aggregates	Fine aggregates	Water
Normal strength concrete	1	0.27	4.4	3.1	0.55

Fig. 2. Tensile test results.

Fig. 4. Moment vs. mid-span deflection of empty steel tubes with different D/t ratios.
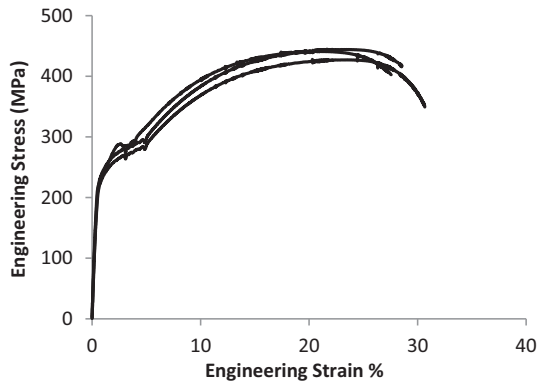
3.1. ST results

The moment vs. the mid-span deflection of the tested ST specimens is illustrated in Fig. 4 for all hollow steel specimens with different D/t ratios. It can be observed that with the decrease of the D/t ratio the flexural capacity increases significantly. It is also observed that despite all the steel tubes failed in a ductile manner, the strain hardening effect was more noticeable for the lowest D/t ratio due to its largest thickness. Besides, the stiffness of the empty tubes increased with the decrease in D/t ratio as shown in Fig. 4. The failure mode, on the other hand, was almost the same for all ST specimens with an inward local buckling at or near the loaded points as illustrated in Fig. 5.

3.2. CFST results

For each D/t ratio, two identical CFST specimens were prepared with the same material and geometric properties, and nearly similar results were obtained for the three different D/t ratios. Fig. 6 compares the load vs mid-span deflection between CFST specimens and the steel tube specimen with the same D/t ratio. The CFST beams were capable of sustaining higher loads as the D/t ratio decreased. For example, specimens with a D/t ratio of 7.82 yielded at around 277 kN as compared to 198 kN and 145 kN for D/t ratios of 13.5 and 17.5 respectively.

The ductile behavior of all CFST beam specimens is quite noticeable in the load-displacement plots of all CFST specimens and no tensile fractures have occurred on the tension flange. In other words, none of the specimens suffered from local buckling or brittle failure. This failure mode which can be seen in Fig. 7 could be attributed to the relatively low D/t ratios for all specimens. In addition, the concrete infill of each specimen was exposed to investigate their failure behavior as seen in
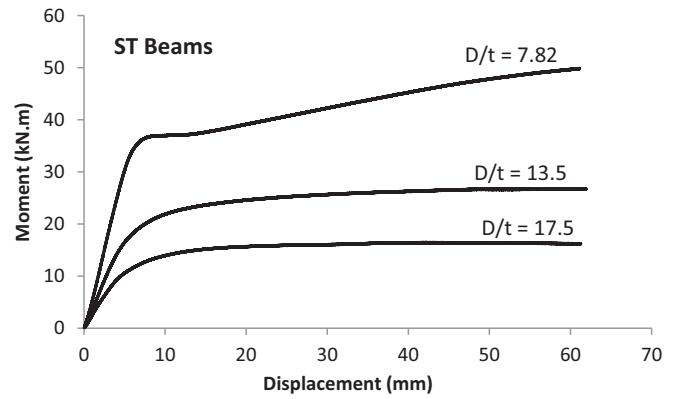

Fig. 5. Failure mode of a hollow steel tube specimen.

Fig. 8. In general, the failure behavior of the concrete infill for all CFST specimens was crushing of the concrete at the compression zone between the two loaded points, while narrow cracks appeared at the soffit of the beam.

The flexural stiffness for specimens with the two higher D/t ratios of 13.5 and 17.5 was almost identical but noticeably lower than the stiffness of the lower D/t ratio of 7.82 as clearly shown in Fig. 9. It can also be concluded from the comparisons of the moment vs displacement results between the three D/t ratios that the flexural capacity of CFST beams increases as the ratio decreases. To exemplify, the moment capacities were 41.53 kN·m, 29.78 kN·m and 21.80 kN·m for D/t ratios of 7.82, 13.5 and 17.5 respectively. The same trend was observed for
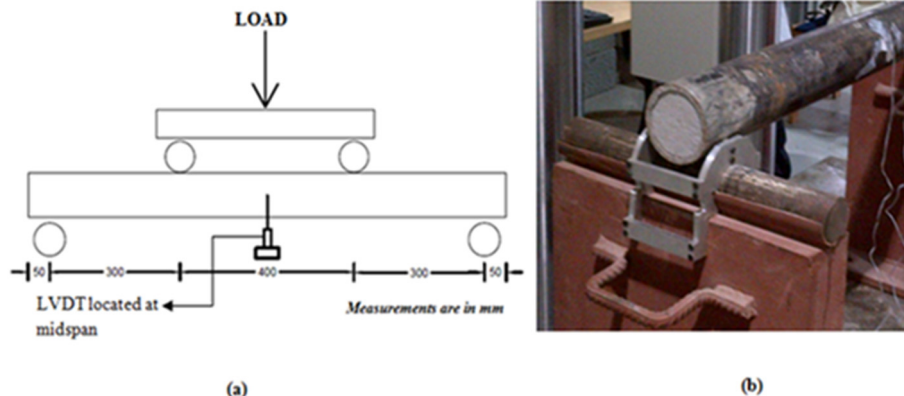

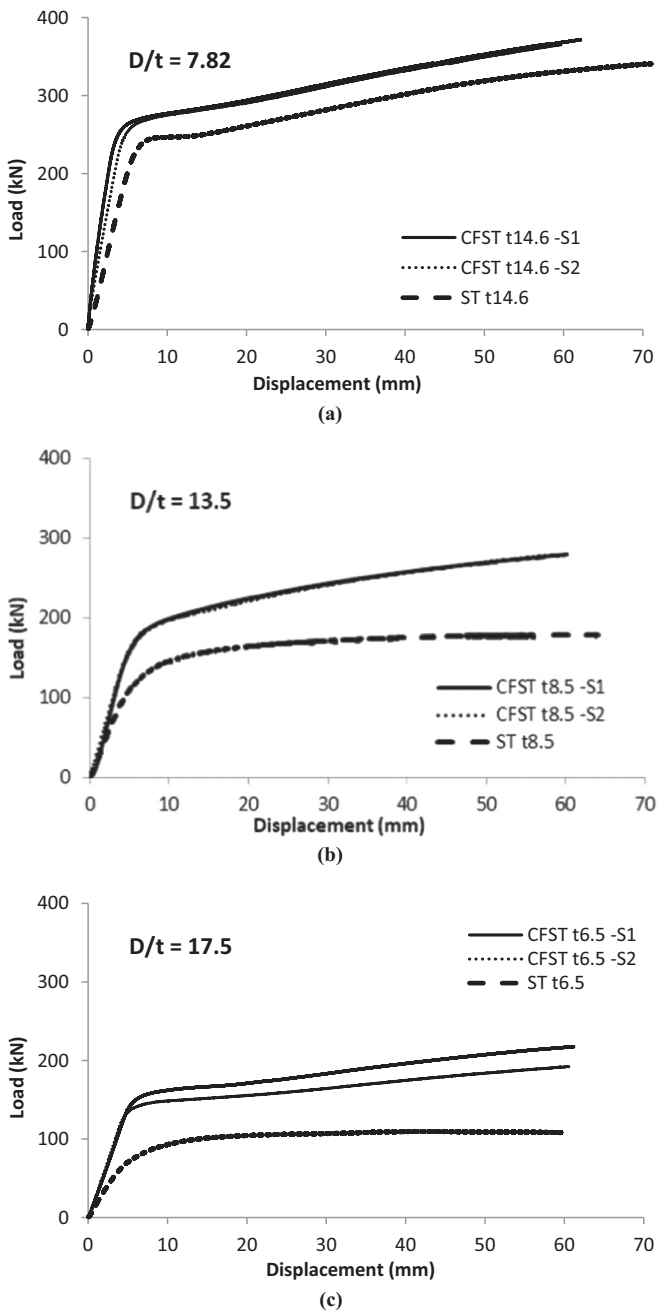Fig. 3. Experimental setup: (a) Test setup, (b) Beam support.

(a)

(b)

(c)

Fig. 6. Load vs. mid-span displacement for specimens with *D/t* ratios of (a) 7.82, (b) 13.5 and (c) 17.5.

the hollow steel tubes (Fig. 4) where the moment capacities were 36.06 kN·m, 22.01 kN·m and 14.32 kN·m, respectively.

The flexural moments versus both the transverse and longitudinal strains encountered at the mid-span for all beams are presented in Fig. 10(a–c). In this paper the moment capacity of CFST specimens is taken as the moment at steel yielding, which is considered at a steel strain of 0.001225. The authors realized from the moment vs strain graphs that the behavior of the tested CFST beams changes from elastic to plastic nearly after the steel reaches the yield strain and the moment beyond this point does not tend to stabilize as strain hardening occurs. Thus, it was difficult to define a certain yield point and it was practical to consider the yield stain of the steel as the point where the CFST beams reach their moment capacity. In addition, local buckling will most likely occur after the yielding of the steel, however, local buckling was not observed for the tested CFST specimens due to the low *D/t* ratios used in this study.
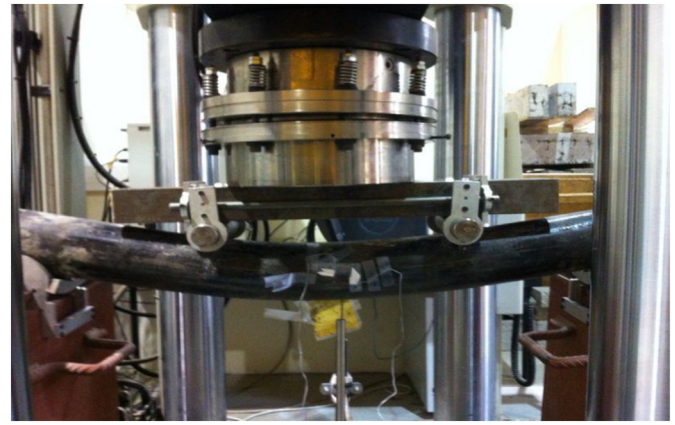

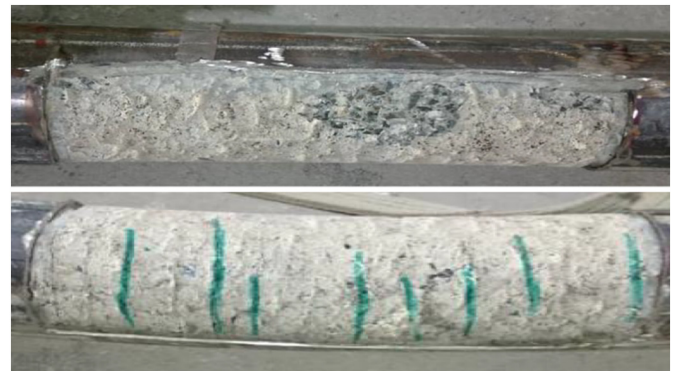**Fig. 7.** CFST beam specimen at ultimate.

Fig. 8. Failure mode of concrete infill at the compression and tension sides.

When comparing the results of the CFST and ST beams in Fig. 10(a–c), it is observed that the CFST beams have a higher stiffness. Both ST and CFST beams sustained mid-span displacements in the range of 60 to 65 mm. However, CFST beams yielded at higher loads. This may be attributed to the additional support provided by the concrete infill which prevents buckling, as well as the additional concrete strength. The difference in the moment capacity between the ST and the CFST specimens decreases as the *D/t* ratio decreases. This can be explained by that as the *D/t* ratio decreases, the steel controls the flexural behavior of the CFST beam and the contribution of the concrete infill to the flexural strength is reduced. However, this can be true only for the
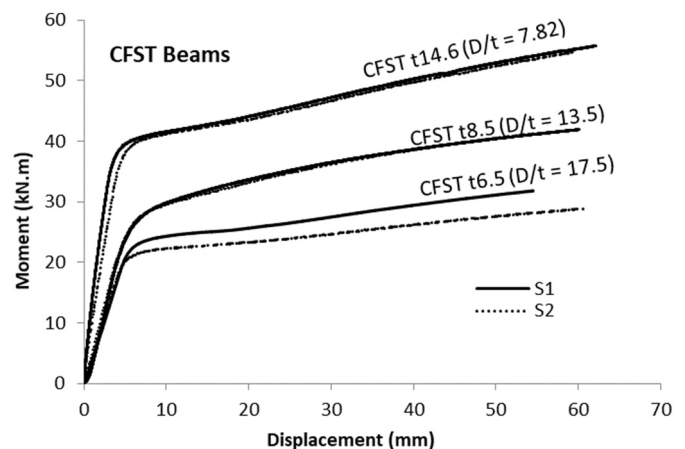

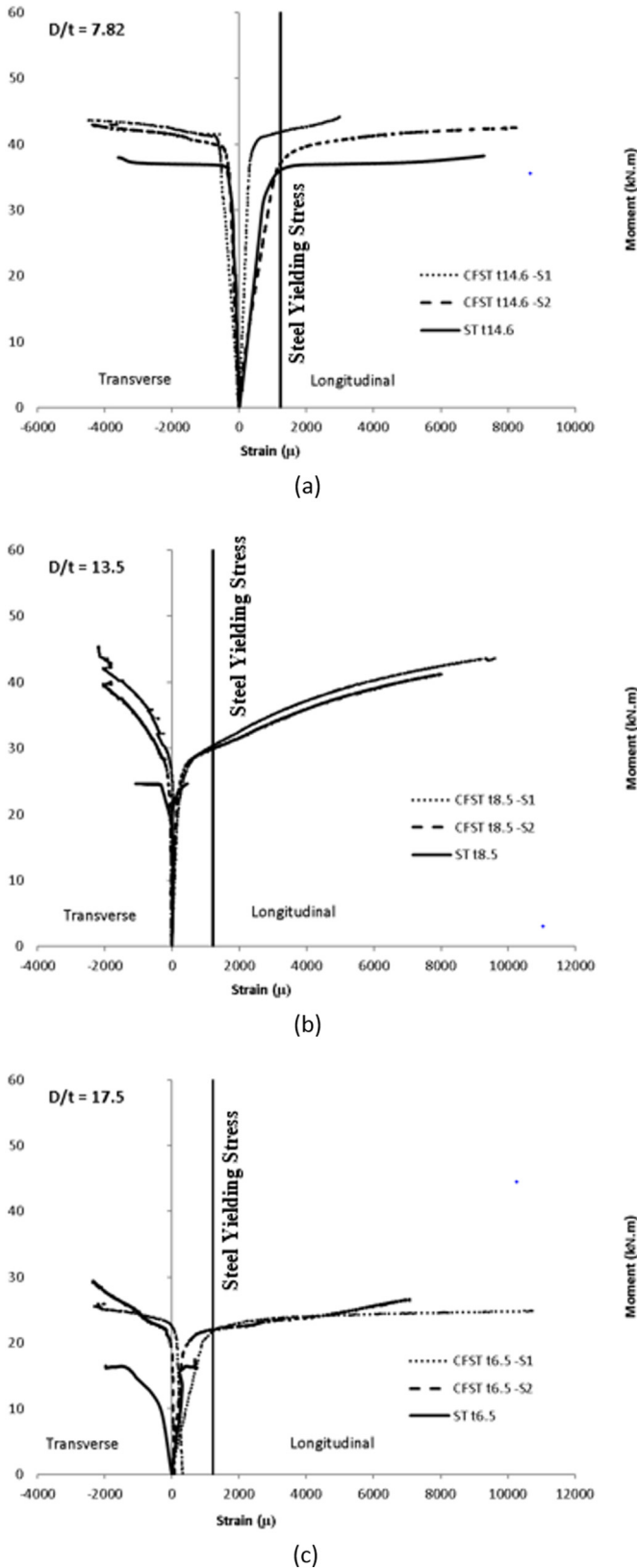**Fig. 9.** Moment vs. mid-span displacement for all CFST beams.

Fig. 10. Moment vs. transverse and longitudinal strains for D/t ratios of (a) 7.82, (b) 13.5 and (c) 17.5.

very small D/t ratios used in this study and further investigation need to be made for larger D/t ratios.

Table 2 summarizes the comparative analysis of CFST and ST beams. The percentage improvement of the flexural strength for CFST beams

increases with D/t ratio. This increase ranged between 15% and 52% for the three D/t ratios considered. On the other hand, the mid-span deflections at yield for all CFST beams were less than those observed in ST beams (Table 2).

4. Theoretical results

The nominal moment M_n of each CFST specimen was calculated based on equations provided by the AISC, AIJ, BS, and EC4 standards as well as analytical equation suggested by Han [3]. Although these standards have studied CFST based on common mechanism, each one has some different assumptions and approaches than others. These common and differences are explained in the following sections. For example, the AISC and AIJ codes use plastic stress distribution method to calculate the flexural capacity of CFST. The AISC also permits the use of strain compatibility method to calculate the flexural capacity. The AIJ code considers the concrete confining effect in calculating CFST flexural capacity. Han proposed an equation to calculate CFST flexural capacity based on regression analysis [3].

4.1. AIJ [17]

The AIJ code discussed composite sections in general and specify a whole chapter to design and analysis of CFST as beam-column member. The flexural capacity of CFST M_n can be calculated by adding the concrete flexural capacity M_n^c to the steel flexural capacity M_n^s as given in Eq. (1). To use this equation, the AIJ code states that the span length of CFST specimen should be <12 times the diameter of steel tube. All of the specimens of this study qualify for this condition (1000 mm < $12 \times 114 = 1368$ mm).

$$M_n = M_n^c + M_n^s \tag{1}$$

The parameters that affect the concrete flexural capacity, include the angular location of the neutral axis, θ_n, concrete diameter, D_c, and the confined strength of concrete, σ_{cB}^c as follows:

$$M_n^c = \sin^3\theta_n \frac{D_c^3 \, \sigma_{cB}^c}{12} \tag{2}$$

The confined strength of concrete is calculated using Eq. (3) which depends on the concrete compressive strength f_c', steel tube thickness, t_s, steel yield strength σ_y^s and diameter of the CFST. A reduction factor of $r_u^c = 0.85$ is also used by the AIJ code.

$$\sigma_{cB}^c = r_u^c \times f_c' \times \frac{1.56 \, t_s \, \sigma_y^s}{D - 2t_s} \tag{3}$$

The flexural capacity of steel tube, M_u^s, is calculated using Eq. (4). AIJ code distinguishes between steel tube part in compression and in tension zones. For compression, AIJ reduces the steel yield strength by the reduction factor $\beta_1 = 0.89$, and increases the steel yield strength in tension by the modification factor $\beta_2 = 1.08$.

$$M_u^s = (\beta_1 + \beta_2) \, \sin\theta_n \frac{\left(1 - \frac{t_s}{D}\right)^2}{2} D^2 t_s \sigma_y^s \tag{4}$$

The moment equation used by the AIJ code could be considered as the most accurate among the other codes as it accounts for the concrete confining effect which helps predicting accurate CFST flexural capacities.

4.2. AISC [11]

The AISC code allows using stress distribution or strain compatibility approaches to calculate the flexural capacity of composite section. It considers load-moment interaction diagrams for CFST and provides equation for each unique point in the interaction diagram. The point

Table 2
Experimental program results.

D/t ratio	CFST moment capacity at yield (kN·m)	ST moment capacity at yield (kN·m)	% Increase in moment capacity	CFST deformation at yield (mm)	ST deformation at yield (mm)	% Decrease in deformation
17.5	21.80	14.32	52.23	7.55	11.21	32.64
13.5	29.78	22.01	35.30	6.62	10.05	34.13
7.82	41.53	36.06	15.17	5.96	8.07	26.14

of pure bending (i.e., zero axial load) is the one that is used to calculate the flexural capacity of CFST, as follows:

$$M_n = F_y Z_s + \frac{1}{2} 0.95 f_c' Z_c \tag{5}$$

where Z_s and Z_c are the plastic modulus of steel and concrete, respectively. AISC does not account for confided concrete since it assumes that CFST behaves as other composite sections. In fact, it reduces f_c' by 5%.

4.3. BS [12]

The BS approach considers the steel plastic section modulus, S, in calculating the CFST flexural capacity, M_n as follows:

$$M_n = 0.91 S f_y (1 + 0.01 m) \tag{6}$$

where the factor (m) is determined using a chart in BS depending on the ratio of concrete cubic strength to steel yield strength for a given D/t ratio. It is clear that BS does not account for confined concrete effect.

4.4. EuroCode4 [13]

Similar to the other codes, EuroCode4 treat CFST as a composite section to determine its flexural capacity. The flexural capacity of CFST, M_n, is calculated by subtracting the neutral moment of CFST, $M_{n. Rd}$, from the maximum moment of CFST, $M_{max. Rd}$, as per the following set of equations:

$$M_n = M_{max} - M_{neut} \tag{7}$$

$$M_{max} = w_{pa} f_y + 0.5 w_{pc} f_c \tag{8}$$

$$M_{neut} = w_{pan} f_y + 0.5 w_{pcn} f_c \tag{9}$$

$$w_{pc} = \frac{(D-2t)^3}{6}; \quad w_{pa} = \frac{D^3 - (D-2t)^3}{6}; \quad w_{pan}$$
$$= D h_n^2 - w_{pcn}; \quad w_{pcn} = (D-2t) h_n^2 \tag{10}$$

where w_{pa} and w_{pc} are plastic moduli of steel tube and concrete, respectively, w_{pan} and w_{pcn} are the plastic moduli of steel tube and concrete at $2h_n$, f_y is the yield strength of steel tube, and f_c is the compressive strength of concrete.

The location of the neutral axis (h_n) is calculated as follows:

$$h_n = \frac{A_c f_c}{2D f_c + 4t \left(2f_y - f_c \right)} \tag{11}$$

4.5. Han [3]

Han proposed two equations for CFST beams; one for square and rectangular cross-sections and the other for circular cross-section. Han's equations were derived based on mechanics of composite and regression analysis as follows:

$$M_n = \gamma_m W_{scm} f_{scy} \tag{12}$$

where $W_{scm} = \pi D^3 / 32$ is the section modulus for circular CFST and f_{scy} is the yield strength of the composite section. Han used regression analysis to determine the flexural strength index (γ_m) and f_{scy} as given by Eq. (13) and Eq. (14), respectively.

$$f_{scy} = (1.14 + 1.02\xi) f_{ck} \tag{13}$$

$$\gamma_m = 1.1 + 0.48 \ln(\xi + 0.1) \tag{14}$$

where the confinement factor ξ is defined in terms of the steel cross-sectional area, A_s, and its yield strength f_{sy} and the concrete cross-sectional area, A_c, and its compressive strength, f_{ck}, as follows:

$$\xi = \frac{A_s f_{sy}}{A_c f_{ck}} \tag{15}$$

4.6. Theoretical results comparisons

The theoretical moment capacity of each specimen was calculated based on equations provided by the AISC, AIJ, BS5400, and EC4 standards and a recent research by Han [3]. Table 3 summarizes the average values of these nominal capacities for each D/t ratio of the CFST beams. Upon comparing the theoretical flexural capacities to their experimental counterparts, all codes provided safe prediction of the moment capacity for all CFST beams considered as illustrated by the flowchart in Fig. 11.

The results predicted by the AIJ code were very close to the experimental values for all D/t ratios considered with not >3% deviation. The moment capacities predicted by the AISC and EC4 codes underestimated the experimental results by a maximum of 9% for the higher D/t ratio of 17.5. The BS, on the other hand, was the most conservative code among the other three standards in which the predicted moment capacities were less than their experimental results by an average of 19%. The reason for that could be attributed to the fact that BS does not account for the concrete confining effect.

The moment capacities predicted by the equation proposed by Han [3] were also compared with CFST experimental results for all cases. For the case of CFST beams with D/t ratios of 13.5 and 17.5, the comparisons show good correlation indicating safe predictions with a
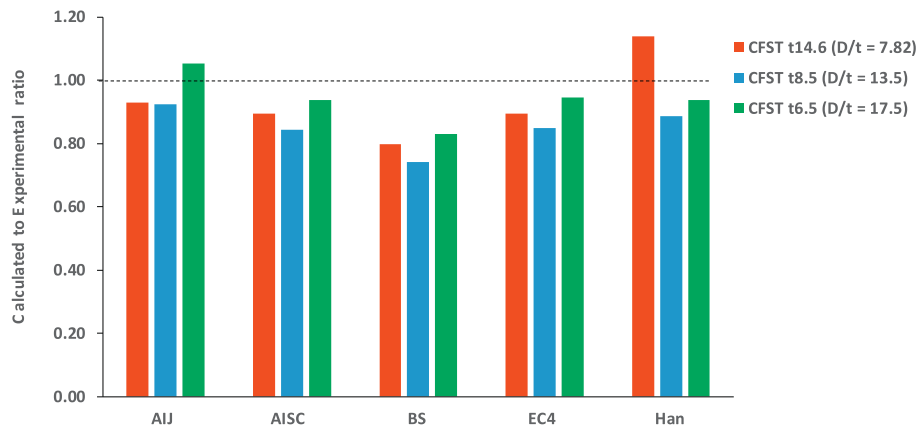
Table 3
Theoretical (Codes) moment capacities for CFST beams.

Beams	M_{AIJ} (kN·m)	M_{AISC} (kN·m)	M_{BS} (kN·m)	M_{EC4} (kN·m)	M_{Han} (kN·m)	M_{Exp} (kN·m)
CFST- D/t = 17.5	22.9	20.5	18.1	20.6	20.4	21.80
CFST- D/t = 13.5	27.5	25.1	22.0	25.2	26.4	29.78
CFST- D/t = 7.82	38.6	37.1	33.2	37.2	47.3	41.53

Fig. 11. Comparison of moment capacities of CFSTs beams with the Codes results.

maximum difference of 7%. However, Han's equation predicted un-conservative moment results for CFST beams with lowest D/t ratio of 7.82. This may be attributed to the inaccurate constants used in his proposed equation. These constants were determined based on regression analysis that was conducted using experimental data for CFST beams with a limited range of D/t ratios. Thus, the experiments presented in this research may add valuable results to the literature and help develop accurate design eqs.

5. FE modeling

A nonlinear finite element model capable of simulating the flexural behavior of CFST specimens was developed using the commercial software ABAQUS. Material and geometric nonlinearities were considered in the developed FE model, taking into consideration the actual elastoplastic stress-strain relationship that was acquired through the experimental program. The experimental results conducted in this study were utilized to verify the FE model which enables studying the flexural behavior of several other CFSTs that have different dimensions, geometries and material properties. In this paper, a description of the steps that was used to develop the nonlinear FE model is discussed and a detailed FE parametric study is presented.

Linear four-node three dimensional (3D) solid elements with reduced integration (C3D8R ABAQUS type) were used to model the concrete infill and the steel tube to simulate the flexural capacity of CFST specimens. The 3D solid element, which has three degrees of freedom per node, provides reliable solution to most applications. Thin to moderately thick-walled structures with large rotation and large strain nonlinearities such as the steel tubes used in this study are typically modeled using 3D shell elements. However, insignificant results deviations were recorded from the shell elements when compared to the solid elements for the CFST beams modeled in this study.

The boundary conditions applied in the FE model reflected approximately the experimental testing setup presented earlier. The end of each CFST specimen was fixed against all translational degrees of freedom except for the displacement at one end in the axial direction of the specimen. The ends are free to rotate in any directions. The BCs were imposed on the CFST beam model either by restraining a set of nodes at the supports locations or by using the coupling approach available in ABAQUS in which the same set of nodes are coupled with a reference point at which the BCs were specified. Though the results were close, the latter approach seems to be more realistic as it accurately describes the ends conditions and the corresponding failure modes. The subjected loads on the CFST specimen were modeled as BCs where a certain displacement was applied at each load location. Fig. 12 gives a geometric description of the FE model for the CFST beams with reference points indicating the locations of supports and loadings.

In the FE modeling, the interaction between the steel tubes and the concrete infill was modeled using surface-to-surface contact, considering both tangential and normal contact definitions with a friction coefficient of 0.3 and tangential angle for concrete of 36°. The option of hard contact was selected to define the normal contact whereas; the penalty method was utilized for the formulation of the tangential friction behavior with finite sliding.

5.1. Materials properties

The material properties for the steel tube are determined using the actual uniaxial stress strain results presented in Fig. 2. Since the analysis involves large strains, the engineering stress–engineering strain results were converted into true stresses-true strains and implemented in the nonlinear FE analysis [18]. In the present 3D FE applications, the flow stress (yield surface) for the steel tube was defined using Isotropic Hardening approach, which is generally considered to be a suitable model for problems in which the plastic straining goes well beyond the incipient yield state (see for more details, Abed and Voyiadjis [17] and Abed [19]).

The nonlinear behavior of the concrete infill was modeled using the Concrete Damaged Plasticity (CDP) Model which uses the concept of isotropic damaged elasticity in combination with isotropic tensile and compressive plasticity to represent the inelastic behavior of concrete. It should be noted that the compressive behavior of concrete would be influenced by the confinement effects provided by the steel tubes. Such an effect was accounted for in the FE model through the definition of the concrete infill material. The properties of the concrete used in the FE model are the same as the tested concrete with an unconfined compressive strength of 39.4 MPa. The stress-strain relationship for the
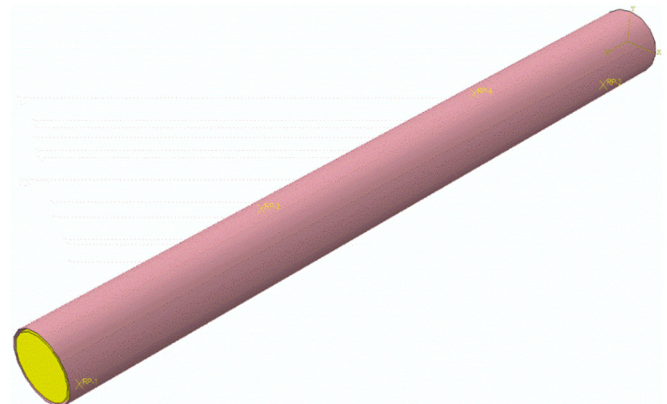

Fig. 12. Assembled CFST beam modeled in ABAQUS using a solid infill and shell tube parts.
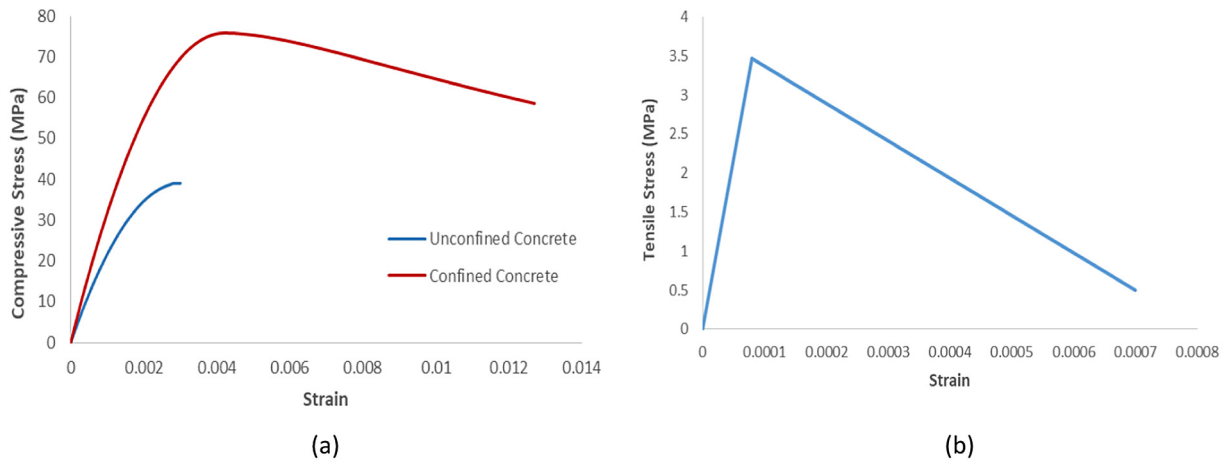
Fig. 13. Equivalent concrete Stress-Strain relationship for (a) Compressive (b) Tensile behaviors.

confined concrete has been established using the equations provided by Ellobody and Young [20] and Montoya [21]. The tensile behavior of the concrete is assumed to be linearly decreasing with the inelastic strain as illustrated in Fig. 13(b). An example of the stress-strain relationship of the compressive behavior of confined and unconfined concrete is presented in Fig. 13(a).

5.2. Mesh sensitivity and model verification

To validate the accuracy of the proposed FE simulations, the flexural capacity and deformation response of a selected CFST beam (CFST t8.5) and steel tube (ST t8.5) were simulated. The load versus displacement results as well as the failure modes were compared with the corresponding experimental results presented in Section 3. To select the proper element size as a first step in FE modeling, mesh sensitivity analysis was conducted by considering three different mesh configurations as shown in Fig. 14. The results of the convergence study indicated that both Mesh3 and Mesh2 converge to similar numerical results as compared with the course Mesh1. In this study, therefore, Mesh2 was selected in the FE modeling of the flexural behavior of CFST and ST beams as it provides accurate results with minimum computational time.
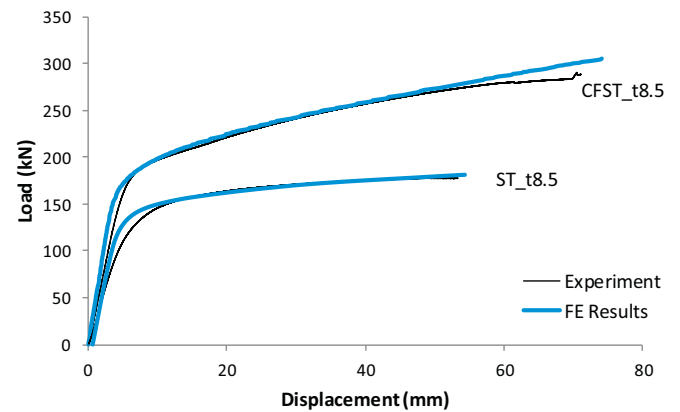

Fig. 15. FE model verifications with experimental results for selected CFST and ST beams.

Load versus displacement results predicted by the proposed FE model showed good comparisons with their experimental counterpart results as demonstrated in Fig. 15. The ultimate capacity predicted by the FE model is relatively close to the experimental results for both CFST and ST beams. However, the FE results produced slightly stiffer results particular at the
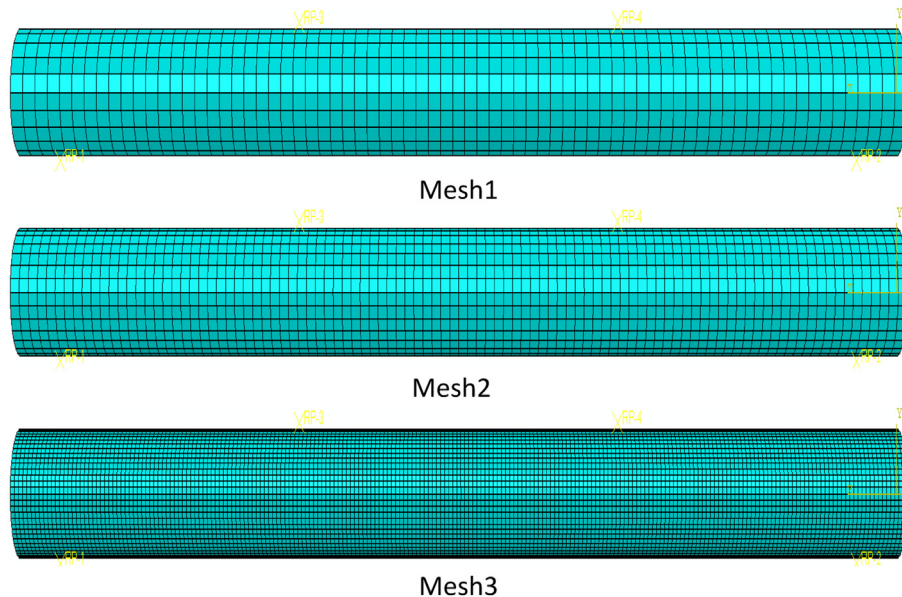

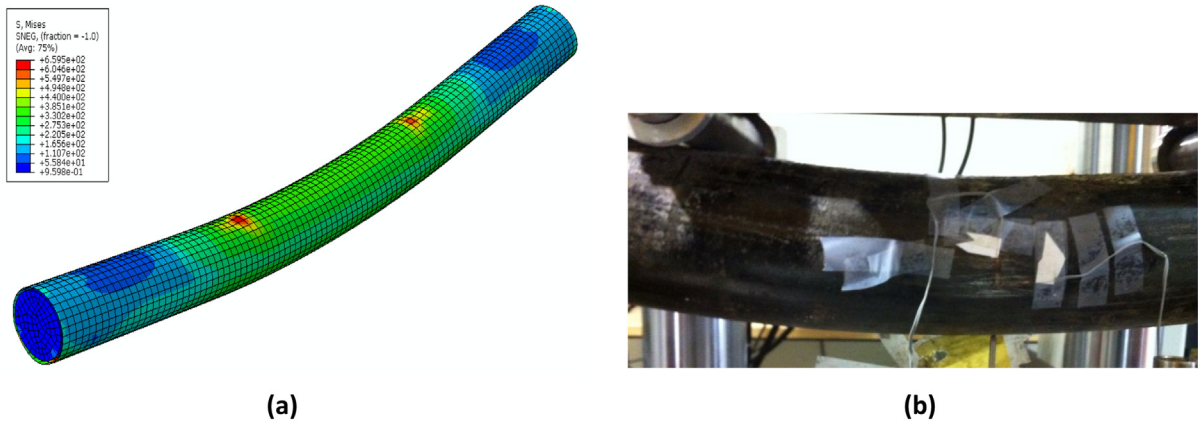**Fig. 14.** Mesh configurations used in the convergence study, Mesh2 was selected.

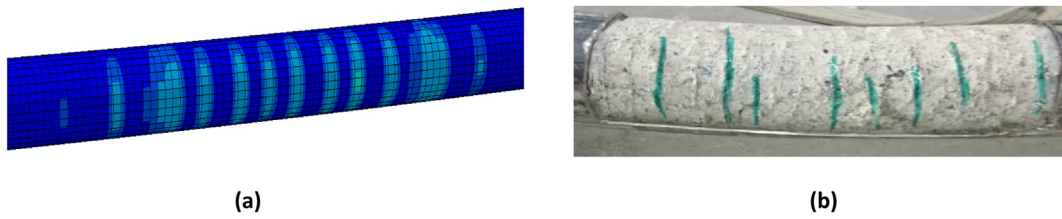**Fig. 16.** Failure modes of CFST beam; (a) FE simulation (b) tested specimen.

Fig. 17. Cracks pattern of concrete infill at the soffit of CFSTs; (a) FE simulation (b) Tested specimen.
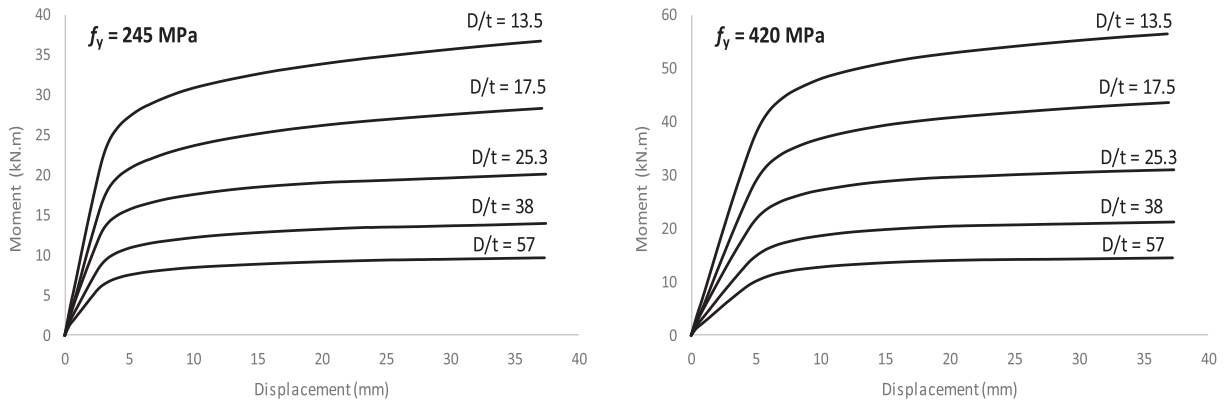

Fig. 18. Effect of the D/t ratio on the flexural behavior of CFSTs for two different yield values.
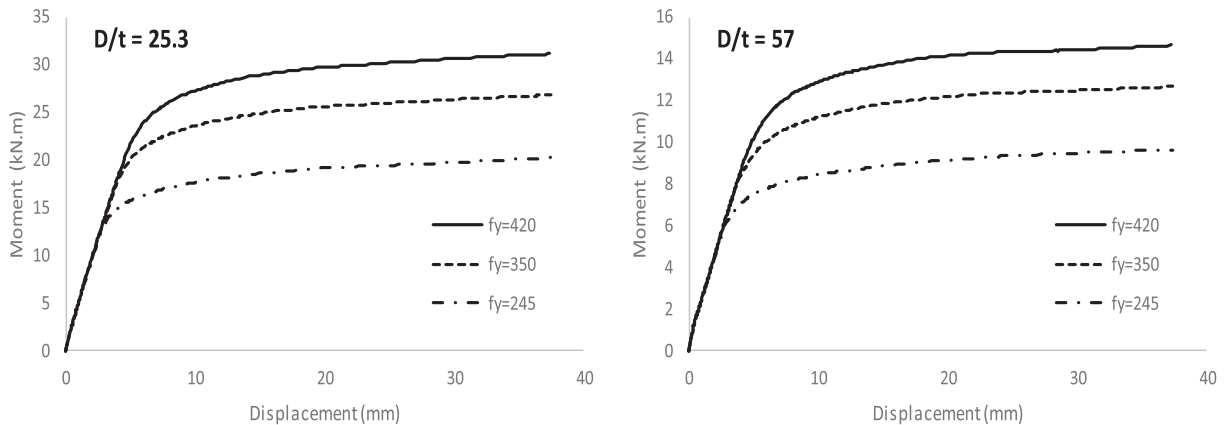

Fig. 19. Effect of steel yield strength on the flexural behavior of CFSTs for two different D/t ratios.

Fig. 20. Comparison between finite element results and codes equations at different D/t ratios and yield strengths.

regions prior to steel yielding. This, in turn, created a slight deviation between the FE results and their experimental counterpart particularly at the transition from the elastic to plastic portions (Fig. 15).

The failure mode for the finite element model was very similar to the experimental observation as none of the specimens suffered from local buckling or brittle failure. The behavior of the CFST specimen in failure was found to be very ductile with high stress concentrations at the locations of the loads as shown in Fig. 16. The deformation capacity of the beams was very large with no tensile fractures occurred at the tension zone of the steel tubes. Fig. 17 also shows comparisons of the cracks patters in the concrete infill at the beam soffit between the FE simulations and the experiments.

Based on the above comparisons, the developed finite element model can further be used to conduct a comprehensive parametric study to examine the effects of the different parameters on the flexural behavior of CFST beams. The parameters that can be included in the parametric study are the material properties (steel and concrete) and the steel tubes shapes and geometry as the flexural behavior of square or rectangular CFSTs can be also investigated.

5.3. Parametric study

In this research, a parametric study was carried out using the above verified FE model to analyze the flexural behavior of seamless CFSTs with a wide range of the D/t ratios (from 13.5 to 57) using one diameter of 114 mm (same diameter as the experimental specimens) and changing the outer tube thickness and yield strengths of the steel tube. The outer tube thicknesses used in this parametric study are 2, 3.5, 4.5, 6.5, and 8.5 mm, the yield strengths are 245, 350, and 420 MPa, and the length of all specimens was 1.1 m. The loading setup was similar to that of the experimental program. From the moment vs mid span deflection curves obtained from the FE model, it can be observed that both the flexural strength and flexural stiffness increase with an increase in the outer tube thickness as shown in Fig. 18, which confirm the present experimental results. In general, it was noticed that the D/t ratio has almost no effect on the plastic behavior of CFST beams where strain hardening occurs. However, the strain hardening is more obvious for beams with low D/t ratio.

Through the analysis of the moment vs mid span deflection relationship of CFST beams with steel yield stresses of 245, 350 and 420 MPa, it was found the that moment capacity of CFSTs beams considerably increases with the increase in the yield stress. Moreover, it was observed that the yield stress does not affect the flexural stiffness of the CFST beams. The moment vs mid span deflection relationship with different f_y (for selected D/t ratios) can be seen in Fig. 19.

Fig. 20 provides a comparison between moment capacities obtained from the FE model and the theoretically calculated using the codes equations provided in Section 4 with different values of D/t ratios and yield strengths (f_y) for the steel tube. The comparison confirmed the previous conclusion (Fig. 11) where the AIJ equations tends to overestimate the moment capacity of CFSTs at higher D/t ratios. It was also found out that the AISC and EuroCode4 equations provide acceptable results for the moment capacity for different D/t ratios and f_y values. Han's equation provided good results for the CFSTs with low D/t ratios, but for the high D/t ratios the results are somewhat conservative. Finally, the results obtained from the BS equation significantly underestimated the moment capacities for all D/t ratios and f_y values.

6. Conclusions

In this paper, the flexural behavior of circular concrete filled seamless steel tubes was investigated experimentally. In general, all CFST beam specimens failed in a ductile mode and no local buckling was observed in any of the specimens. The moment capacity of the CFST beam specimens increased as compared to empty beams (STs). However, this increase was more significant for higher D/t ratios. CFST section with low D/t ratio behaves more like a bare steel section and the contribution of the concrete infill to the flexural capacity would be very small or negligible.

The moment results obtained from the experimental program were also compared with well-known international design codes such as the AIJ, AISC, BS540 and the Eurocode4 as well as with the theoretical values predicted by Han's equation. For the CFST specimens considered, the BS significantly underestimated the experimental flexural capacities while the AISC and EuroCode4 predicted reasonably conservative moments and the AIJ code provided very close results. Han's equation provides a good method to estimate the flexural strength of CFSTs. However, it cannot be recommended to predict the flexural capacity of CFSTs with low D/t ratios.

The flexural behavior of circular CFST beams was also investigated numerically by developing a nonlinear 3D finite element model using the commercial software ABAQUS. The FE mode included material and geometric nonlinearities and was validated using the experimental results. A very good agreement was achieved between the finite element simulation and the experimental results in terms of the moment capacity, the plastic behavior, the failure mode and the moment-deflection curves for all tested specimens. The developed finite element model was used to conduct a parametric study to further investigate the flexural behavior of seamless CFSTs considering higher D/t ratios and different steel yield strengths. Both the experimental and the FE results showed that the flexural capacity of circular CFST beams significantly increases with the decrease in the D/t ratio, while all beams have a very similar ductile behavior regardless of the D/t ratio. In addition, the FE results showed that the flexural strength and stiffness are significantly affected by the D/t ratio, while the steel yield strength only affects the flexural strength.

It should be mentioned that the above conclusions are limited to the parameters used in this study. The experimental part of this study included CFST beams of a diameter of 114 mm with three different D/t ratios (7.82, 13.5 and 17.5) and a steel yield strength of 245 MPa. In addition, the FE parametric study was carried out using CFST beams with the same diameter (114 mm) but with a wider range of D/t ratio (13.5 to 57) and yield strengths (245 to 420 MPa) to expand the research scope. Additional experimental tests on seamless CFST beams considering different tube diameters, larger D/t ratios, higher steel yield strengths and different concrete grades are recommended.

References

[1] J. Moon, C.W. Roeder, D.E. Lehman, H.-E. Lee, Analytical modeling of bending of circular concrete-filled steel tubes, Eng. Struct. 42 (2012) 349–361.

[2] W.R. Charles, E.L. Dawn, B. Erik, "Strength and Stiffness of Circular Concrete-Filled Tubes," 2010/12/01, 2010.

[3] L.-H. Han, "Flexural behaviour of concrete-filled steel tubes," J. Constr. Steel Res., Vol. 60, 2, 313–337, 2004.

[4] A.D. Probst, T.H.-K. Kang, C. Ramseyer, U. Kim, Composite flexural behavior of full-scale concrete-filled tubes without axial loads, J. Struct. Eng. 136 (11) (2010) 1401–1412.

[5] F. Abed, M. AlHamaydeh, S. Abdalla, Experimental and numerical investigations of the compressive behavior of concrete filled steel tubes (CFSTs), J. Constr. Steel Res. 80 (2013) 429–439.

[6] S. Abdalla, F. Abed, M. Alhamaydeh, Behavior of CFSTs and CCFSTs under quasi-static axial compression, J. Constr. Steel Res. 90 (2013) 235–244.

[7] F.H. Abed, M.A. Najib, A.K. Ilgun, Flexural Behavior of Concrete Filled Seamless Steel Tube (CFST) Beams, 2015.

[8] S. Arivalagan, S. Kandasamy, Finite element analysis on the flexural behaviour of concrete filled steel tube beams, J. Theor. Appl. Mech. 48 (2) (2010) 505–516.

[9] L.-H. Han, W. Li, R. Bjorhovde, Developments and advanced applications of concrete-filled steel tubular (CFST) structures: members, J. Constr. Steel Res. 100 (2014) 211–228.

[10] B.B. Colin, W.R. Charles, C. Brad, "Composite Action in Concrete Filled Tubes," 2017/01/23, 1999.

[11] G. Hanbin, U. Tsutomu, "Strength of Concrete-Filled Thin-Walled Steel Box Columns: Experiment," 2017/01/25, 1992.

[12] A. Committee, Specification for Structural Steel Buildings (ANSI/AISC 360-10), American Institute of Steel Construction, Chicago-Illinois, 2010.

[13] B. Standard, BS5400 Steel, Concrete and Composite Bridges, Part 5, Code of Practice for the Design of Composite Bridges, British Standard Institution, 2005.

[14] C.E. de Normalisation, Eurocode 4: Design of Composite Steel and Concrete Structures. Part 1-2: General Rules-Structural Fire Design, CEN ENV, 1994.

[15] M. Elchalakani, X. Zhao, R. Grzebieta, Concrete-filled circular steel tubes subjected to pure bending, J. Constr. Steel Res. 57 (11) (2001) 1141–1168.

[16] R. Wang, L.-H. Han, J.-G. Nie, X.-L. Zhao, Flexural performance of rectangular CFST members, Thin-Walled Struct. 79 (2014) 154–165.

[17] A. I. o. J. (AIJ), "Recommendations for design and construction of concrete filled steel tubular structures," ed, October 1997.

[18] F.H. Abed, G.Z. Voyiadjis, Plastic deformation modeling of AL-6XN stainless steel at low and high strain rates and temperatures using a combination of bcc and fcc mechanisms of metals, Int. J. Plast. 21 (8) (2005) 1618–1639.

[19] F.H. Abed, Constitutive modeling of the mechanical behavior of high strength ferritic steels for static and dynamic applications, Mech. Time-Depend. Mater. 14 (4) (2010) 329–345.

[20] E. Ellobody, B. Young, D. Lam, Behaviour of normal and high strength concrete-filled compact steel tube circular stub columns, J. Constr. Steel Res. 62 (7) (2006) 706–715.

[21] E. Montoya, F.J. Vecchio, S.A. Sheikh, Compression field modeling of confined concrete: constitutive models, J. Mater. Civ. Eng. 18 (4) (2006) 510–517.